Journal of Materials Chemistry C

Accepted Manuscript

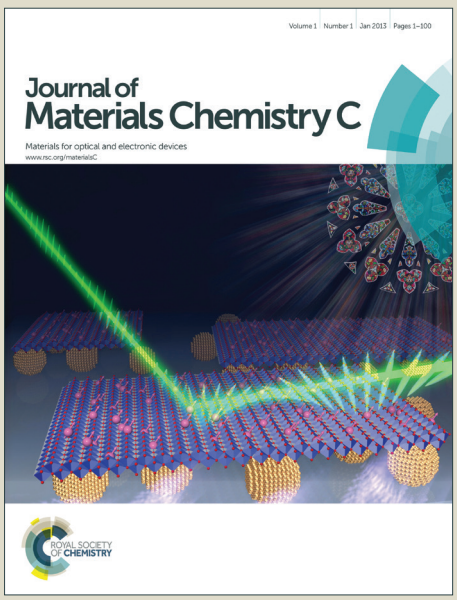

ROYAL SOCIETY OF CHEMISTRY

www.rsc.org/materialsC

Journal of Materials Chemistry C

Journal of Materials Chemistry C

Dynamic Article Links ►

Cite this: DOI: 10.1039/c0xx00000x

www.rsc.org/xxxxxx

ARTICLE TYPE

New Multifunctional Phenanthroimidazole-Phosphine Oxide Hybrids for High-Performance Red, Green and Blue Electroluminescent Devices

Kai Wang, Shipan Wang, Jinbei Wei, Shanyong Chen, Dong Liu, Yu Liu* and Yue Wang*

Received (in XXX, XXX) Xth XXXXXXXXX 20XX, Accepted Xth XXXXXXXXX 20XX

DOI: 10.1039/b000000x

In this work, two novel electron-accepting phosphine oxide moiety attaching phenanthroimidazole hybrids have been designed and synthesized. The P=O group is used as a point of saturation between the PPI moiety and the outer phenyl groups, so the high triplet energy of PPI is preserved to act as host for red and green phosphorescent dopants. The strong intermolecular interactions and steric effect of diphenylphosphine oxide (DPO) moiety endows the films with high quantum yields in deep blue emission region. Compared to PPI, the carrier (hole- and electron-) injection/transport properties were greatly promoted by the appendent DPO group through single carrier devices measurement. Besides, the morphological and thermal stabilities were also improved. The multifunction enables adaptation of several simplified device configurations. The non-doped deep-blue fluorescent device exhibits external quantum efficiency of 2.24% with CIE (0.16, 0.08), very close to NTSC blue standard CIE (0.14, 0.08). High-performance green (65.4 cd A^{-1}, 73.3 lm W^{-1} and 18.0%) and red (19.0 cd A^{-1}, 21.3 lm W^{-1} and 13.5%) phosphorescent devices using them as hosts have been achieved. The relationship between molecular structures and optoelectronic properties is discussed experimentally and theoretically.

Introduction

Organic light-emitting diodes (OLEDs) have attracted considerable scientific and industrial interests since the pioneering work by Tang et al. in 1987.[1] Extensive research has been made to promote OLEDs into commercial applications as full-color flat-panel displays and solid-state lighting sources.[2] During the last two decades, many new emitters with red (R)[3], green (G)[4] and blue (B)[5] emission and hosts have been developed for full color and WOLEDs.[6] Accompany with HTL and ETL materials, at least six kinds of organic materials or more were needed to achieve full-color display. In addition, the optimized device structures of various color are usually different. Therefore, the full-color OLEDs and WOLEDs are often established based on a complex material system, high cost organic syntheses and complicated device fabrication. In this sense, with an aim to reduce the production cost of materials and simplify the manufacturing process, achieving high-performance full color electroluminescence based on a simple material system and device structure becomes an important issue for OLED applications. In principle, a blue emitter with balanced carrier transport characteristic and high triplet energy (E_T) may be employed as host for green and red phosphors, which can solve the problem. Lots of efforts have been put to the development of new types of blue fluorescent emitters as well as phosphorescent host.[7] Recently, we reported two metal-phenanthroimidazole derivatives with ambipolar transport[8] and small singlet-triplet splitting property and we realized highly efficient R, G and B electroluminescent devices based on them.[9] Herein, we report the design and synthesis of two new 1,2-diphenyl-phenanthroimidazole (PPI)-diphenylphosphine oxide (DPO) hybrids with *meta* linkages, namely DPO-PPI and DPO-2PPI. Although a lot of hosts bearing DPO skeleton have been reported, the study of using them as emitters is seldom.[10] The DPO group doesn't extend the π conjugation of the chromophore (PPI) and thereby retains its high T_1 levels, while the fluorescent emission in films of them changes from violet of PPI to deep blue due to the strong P-O···H-C and C-H···π intermolecular interactions present in crystal.[11] The fluorescent quantum yields and thermal stability have been enhanced. Meanwhile, it could efficiently polarize the molecules to make contributions to the lowest unoccupied molecular orbital (LUMO) and greatly improves carrier injection/transporting ability.[12,13] The influence on chemical, physical and electronic properties of the introduction of DPO moiety has been carefully studied. The relationship between their structures and properties is discussed experimentally and theoretically. Based on these multifunctional materials, good color purity deep-blue fluorescent, red and green phosphorescent devices with simplified structures were fabricated and shown remarkable performances.

Results and discussion

Synthesis, characterization and crystal

1-phenyl-2-(3-(diphenylphosphineoxide)phenyl)-1*H*-phenanthro[9,10-*d*]imidazole (DPO-PPI) was synthesized from 2-(3-bromophenyl)-1-phenyl-1*H*-phenanthro[9,10-*d*]imidazole by treatment with *n*-butyllithium, followed by

chlorodiphenylphosphine to give the corresponding phosphine product. Afterwards, oxidation of the phosphine precursor with H_2O_2 produced DPO-PPI with an overall yield of 63% (Scheme 1). Compound DPO-2PPI was synthesized by a similar procedure except that dichloro(phenyl)phosphine was used as the reactant instead of chlorodiphenylphosphine with an overall yield of 44% (see experiment for details). Both the compounds were then purified by temperature-gradient sublimation under vacuum conditions before measurements and device fabrication processes. They were fully characterized using ^{1}H NMR spectra, mass spectrometry and elemental analysis. The molecular structure of DPO-PPI was further determined by single-crystal analysis.

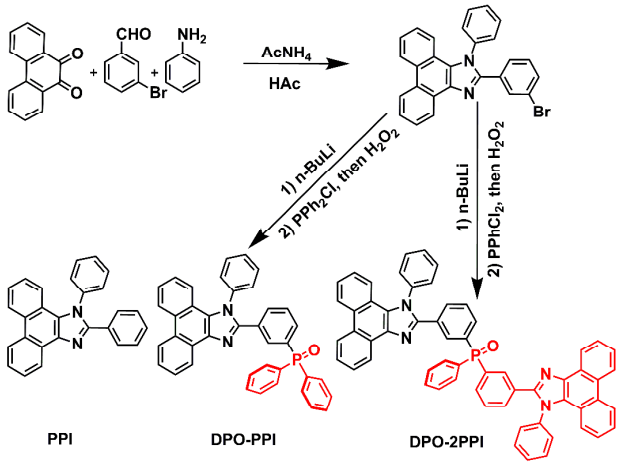

Scheme 1 Synthetic procedure and structures of PPI, DPO-PPI and DPO-2PPI.

The X-ray crystallography of DPO-PPI revealed that the crystal structure belongs to monoclinic space group P2(1)/c with Z=4. The DPO moiety and benzene ring attaching on the 2-position imidazole adopt approximate tetrahedral geometry centring P atom (Figure 1a). Adjacent phenanthroimidazole units are stacked approximately parallel and assemble in the crystal lattice along the *a* axis *via* intermolecular edge-to-face C–H···πinteractions (d = 2.71 Å; θ = 154.5°, C–H bond belongs to the benzene ring of DPO moiety and π cloud is the PPI plane, green lines in Figure 1b) to generate a molecular chain, and this line is further stabilized by C–H···π interactions (d = 2.92 Å; θ = 148.7°, C–H bond belongs to benzene ring attaching on the 1-position imidazole and π cloud is the PPI plane, red lines in Figure 1b). Besides, every three DPO-PPI molecules are interlinked through hydrogen-bonding interactions with one water molecule to form a 3D networks. No π···π stacking exists between neighbor molecules owing to the strong steric-inhibition effect of DPO moiety. These intermolecular interactions observed in the crystal might be beneficial to charge carrier mobility.

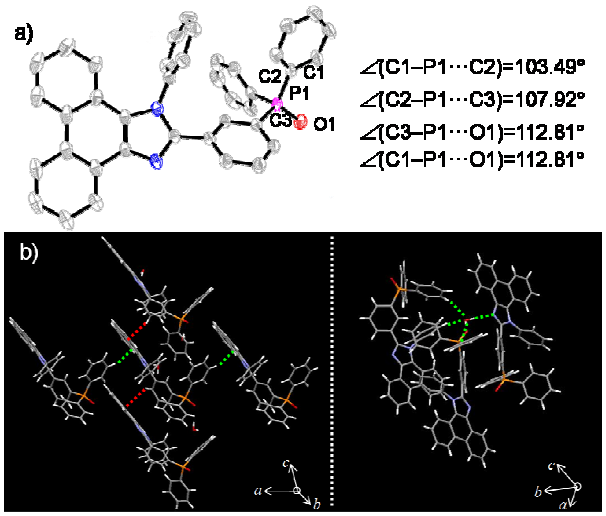

Fig. 1 (a) molecular structure of DPO-PPI with 50% probability level. Hydrogen atoms are omitted for clarity. Selected bond angles. (b) packing structure of DPO-PPI.

Thermal Properties and Theoretical Calculations

The thermal properties of the compounds were characterized by thermogravimetric analysis (TGA) and differential scanning calorimetry (DSC) under a nitrogen atmosphere at a heating rate of 10 °C/min (Figure 2). In the TGA measurements, both DPO-

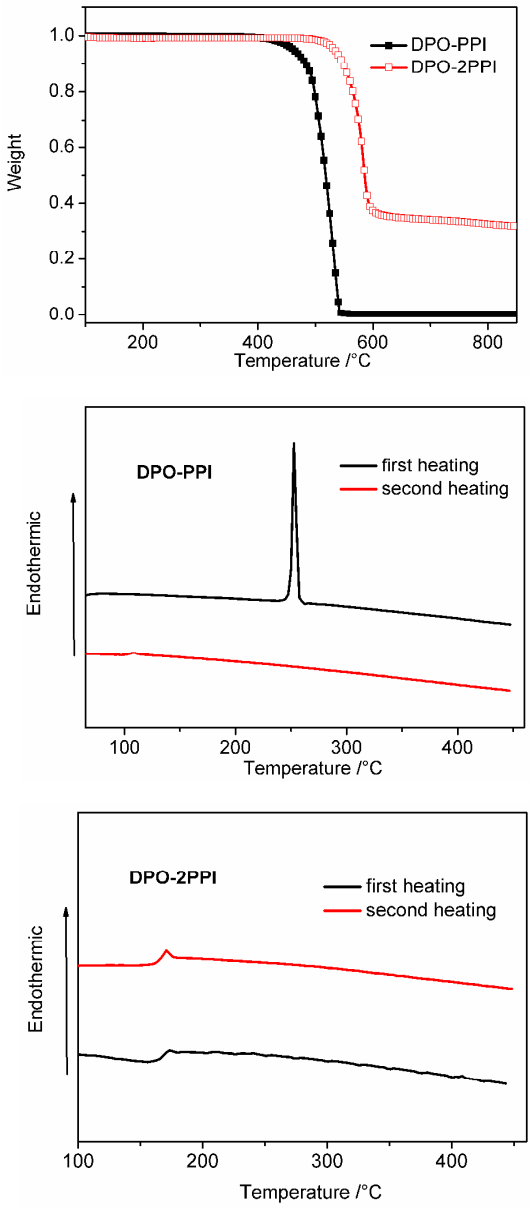

Fig. 2 TGA and DSC thermograms of DPO-PPI and DPO-2PPI

PPI and DPO-2PPI exhibited high decomposition temperatures (T_{d5}, corresponding to 5% weight loss) at 463 and 533 °C, respectively. The glass-transition temperatures (T_g) of DPO-2PPI (173 °C) is higher than that of DPO-PPI (109 °C) due to its increased molecular size and molecular weight.[14] Compound DPO-PPI shows melting point (T_m) at 252 °C in the first heating process, while compound DPO-2PPI doesn't show endothermic peaks corresponding to melt during the two heating processes, which is indicative of unique glassy state of them. As a consequence, the new compounds can form homogeneous and stable films upon thermal evaporation.

The influence of DPO moiety substitution on the frontier molecular orbitals of DPO-PPI and DPO-2PPI was investigated by DFT calculations (Figure 3). Because the P=O group acts as a point of saturation and prevents electronic communication between the PPI unit and outer two benzene rings, the molecular orbitals distribution of DPO-PPI and DPO-2PPI are quite similar to that of PPI. So the photophysical properties of DPO-PPI and DPO-2PPI are expected to be representative of PPI. The highest occupied molecular orbitals (HOMO) of them were almost located on phenanthroimidazole group and the linked benzene ring. For the lowest unoccupied molecular orbitals (LUMO), the *N*-phenyl ring makes a moderate contribution on PPI but makes no contribution on DPO-PPI and DPO-2PPI. Small amount of LUMO of DPO-PPI and DPO-2PPI is located on the benzene ring of DPO moiety. They both exhibit partial separation of the HOMO and LUMO levels. The strong inductive influence of the P=O group is predicted to lower LUMO by 0.16 eV, which favours the electron injection from the cathode.

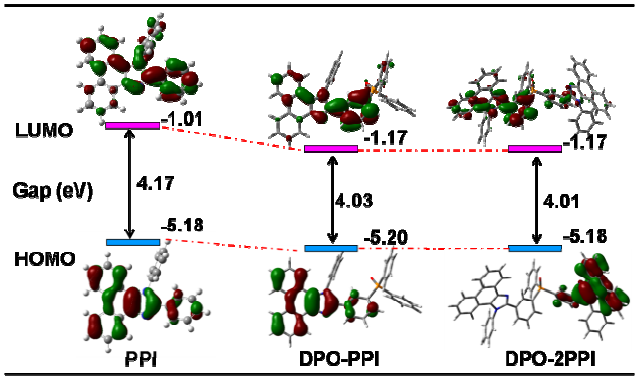

Fig. 3 Calculated molecular orbitals and energy levels of the compounds.

Photophysical Properties

The UV/vis absorption spectra and photoluminescent (PL) spectra of DPO-PPI and DPO-2PPI in CH_2Cl_2 (10^{-5} mol L^{-1}) and films are shown in Figure 4. For comparison, we measured the photophysical property of PPI under the same conditions (Figure S1). The absorption spectra and PL spectra in solution of them were nearly the same as PPI, indicating the appendent DPO moiety doesn't extend the conjugated length, which is in accord with the DFT calculation result. The emission of thermal evaporated film exhibited broad and structureless band with bathochromic shifts of the maximum peaks by 35 and 30 nm compared to PPI, respectively. This should be ascribed to the aggregation formation induced by P–O···H–C and C–H···π intermolecular interaction, which is revealed in common for phosphine oxides[11]. Their fluorescent quantum yield (Φ_f) in dilute solution (10^{-5} M) is 0.94 for DPO-PPI and 0.91 for DPO-2PPI, and those in film is 0.57 for DPO-PPI and 0.55 for DPO-2PPI, indicating both compounds are promising candidates as deep-blue emitters in OLEDs. The phosphorescence spectra were measured in the 2-MeTHF solution (10^{-5} M) at 77 K. Their triplet energy E_T estimated from the highest-energy vibronic sub-band is 2.57 and 2.55 eV, respectively, these values are slightly smaller than PPI (2.61 eV) and sufficiently high to be used as host for green and red phosphorescent emitters.

Electrochemical Properties

Cyclic voltammetry (CV) was performed to investigate the electrochemical properties of the compounds. As shown in Figure 5, the three compounds exhibit similar reversible, one-electron oxidation process, which can be assigned to the oxidation of phenanthroimidazole moiety. The HOMO and LUMO energy levels of the compounds were determined from the onset of the oxidation and reduction potentials with regard to the energy level of ferrocene (5.1 eV[15] below vacuum). The estimated HOMO levels are –5.90 eV (DPO-PPI) and –5.94 eV (DPO-2PPI), similar to PPI (–5.87 eV). The estimated LUMO levels are –2.66, –2.70 and –2.37 eV for DPO-PPI, DPO-2PPI and PPI, respectively.

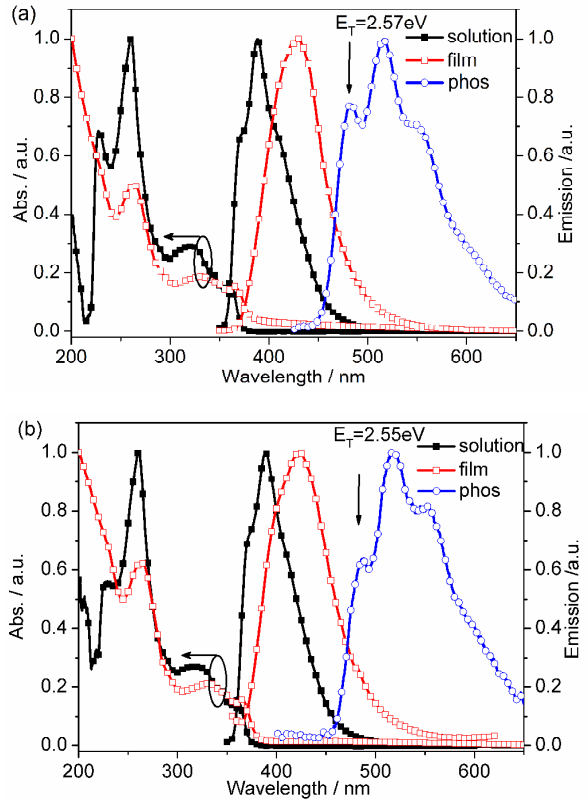

Fig. 4 Room-temperatrue UV-vis absorption spectra, PL spectra of DPO-PPI (a) and DPO-2PPI (b) in CH_2Cl_2 solution (10^{-5} M) and neat films, as well as their phosphorescence spectra in 2-MeTHF solution (10^{-5} M) at 77K.

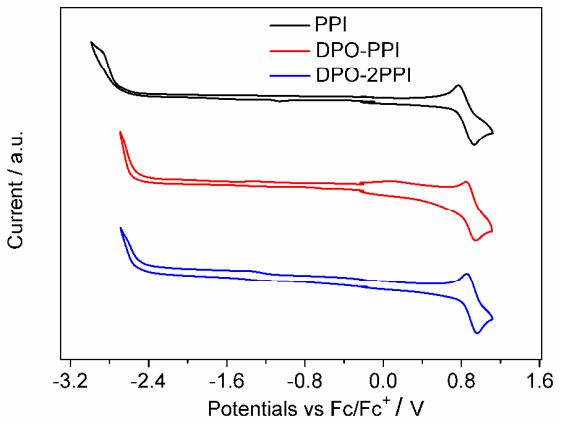

Fig. 5 Cyclic voltammograms of PPI, DPO-PPI and DPO-2PPI in CH_2Cl_2/DMF for oxidation and reduction, respectively.

Table 1 Summary of Physical Properties of DPO-PPI and DPO-2PPI

Compound	λ_{abs}/nm sol[a]/film	λ_{em}/nm sol[a]/film	Φ_F/ sol[a]/film	HOMO/LUMO /eV	T_g/T_{d5} ºC
DPO-PPI	361/365	389/429	0.94/0.57	–5.90/–2.66	109/463
DPO-2PPI	362/365	388/424	0.91/0.55	–5.94/–2.70	173/533

[a] Concentration: 1.0×10^{-5} M in CH_2Cl_2 solution

Single-Carrier Devices

Single-carrier devices of the three compounds with the structures of [ITO/MoO_3 (10 nm)/ compound (60 nm)/MoO_3 (10 nm)/Al (100 nm)] for hole-only device and [ITO/TPBI (10 nm)/ compound (60 nm)/ TPBI (10 nm) /LiF (1 nm)/Al (100 nm)] for electron-only device were fabricated (Figure 6). MoO_3 and TPBI layers are used to prevent electron and hole injection from the cathode and anode, respectively.[13f,16] The *I–V* characteristics of single-carrier devices documented that both hole and electron current densities are greatly increased compared to PPI, suggesting the pendent DPO moiety greatly improved the carrier injection/transport ability of PPI. Compared to the typical electron-transport moiety benzimidazole, phenanthroimidazole keeps its good electron injection ability and improves the hole injection ability. Therefore, phenanthroimidazole has relatively balanced hole and electron injection/transport ability, as shown in Figure 6a, 6b and other research before.[5m] DPO moiety is an electron-transporting group, so it improves the electron injection/transport ability of PPI. The introduction of phosphine oxide moiety induce more separated HOMO and LUMO orbital of the two compounds, which could provide respective transporting channel for hole and electron and thus benefits the efficient hole- and electron-transport properties.[17] Besides, the carrier transporting properties of organic semiconductors are very sensitive to molecular structure, molecular configuration as well as molecular packing modes in solid state. Through comparison between the emission of film and solution, there is moderately intermolecular interaction in the thermal evaporated film. This is favorable to the hole and electron injection/transport.[18] Overall, both of them exhibit bipolar transport abilitiy after appending phosphine oxide moiety and the electron injection/transport abilities improve more than their hole injection/transport abilities. It is worth noting that both DPO-PPI and DPO-2PPI exhibit relatively balanced hole and electron current density, which is crucial in achieving high efficiency and low roll-off OLEDs. In addition, the hole current densities of the two compounds are similar while the electron current density of DPO-2PPI is slightly higher than DPO-PPI. We attributed this for the following reason:

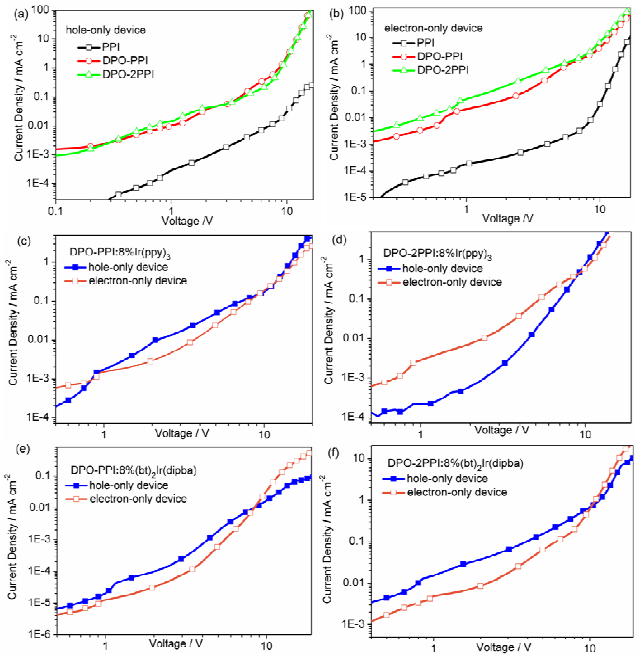

Fig. 6 Current density versus voltage characteristics of the hole-only (a) and electron-only (b) devices for DPO-PPI, DPO-2PPI and PPI. *J-V* curves of DPO-PPI (c) doped with 8wt% $Ir(ppy)_3$, DPO-2PPI (d) doped with 8wt% $Ir(ppy)_3$, DPO-PPI (e) doped with 8wt% $(bt)_2Ir(dipba)$ and DPO-2PPI (f) doped with 8wt% $(bt)_2Ir(dipba)$.

1) the slightly lower LUMO energy level of DPO-2PPI compared to that of DPO-PPI indicates its smaller injection barrier; 2) the more separated HOMO and LUMO of DPO-2PPI compared to that of DPO-PPI could be more favourable to hole- and electron-transport. As we know, the doped molecules would influence charge transport of the film, so we fabricated the single-carrier devices of doping films of the two compounds (Figure 6). Both the hole and electron currents are greatly decreased when doping $Ir(ppy)_3$ or $(bt)_2Ir(dipba)$ into the hosts, indicating that the doped iridium complex act as roles of carrier trapping sites.[19] But overall, they still show relatively balanced carrier transport and the current density of film based on DPO-2PPI is slightly higher than that of DPO-PPI.

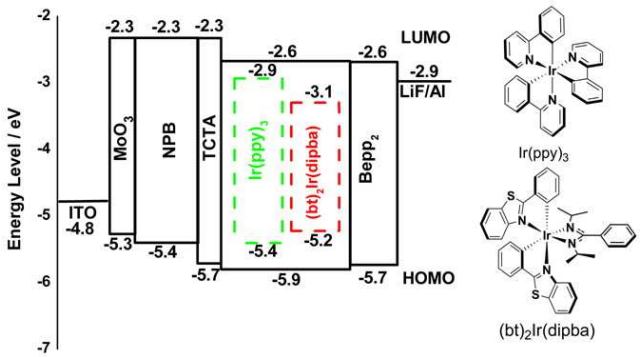

Fig. 7 Energy level diagram of the materials used and the chemical structures of the phosphorescent materials.

Undoped Deep-Blue OLEDs

We initially examined the performance of non-doped deep blue-emitting devices with the structure of [ITO/MoO_3 (10 nm)/NPB (30 nm)/TCTA (5 nm)/DPO-PPI or DPO-2PPI (25 nm)/$Bepp_2$ (60 nm)/LiF (1 nm)/Al (100 nm)] (device **B1** with emitting layer composed of DPO-PPI and device **B2** with emitting layer composed of DPO-2PPI). In devices **B1** and **B2**, 1,4-bis[(1-naphthylphenyl)amino]-biphenyl (NPB) was used as the hole-transport material, 4,4′,4″-tri(*N*-carbazolyl)triphenylamine (TCTA) was used as the electron-blocking layer, as well as triplet exciton blocker layer in the PhOLEDs, bis(2-(2-hydroxyphenyl)-pyridine)beryllium ($Bepp_2$) was utilized as the electron-transport material, MoO_3 and LiF served as hole- and electron-injecting layer, respectively. Devices **B1** and **B2** exhibit deep-blue emissions with Commission International de l'Eclairage (CIE) coordinates of (0.16, 0.09) and (0.16, 0.08), respectively, which are very close to the NTSC (National Television Standards Committee) blue standard (CIE: 0.14, 0.08) and remain almost unchanged over a wide range of driving voltage. Device **B2** using DPO-2PPI as emitter exhibited a turn-on voltage of 3.4 V. The maximum external quantum ($\eta_{ext.max}$), current ($\eta_{c.max}$) and power

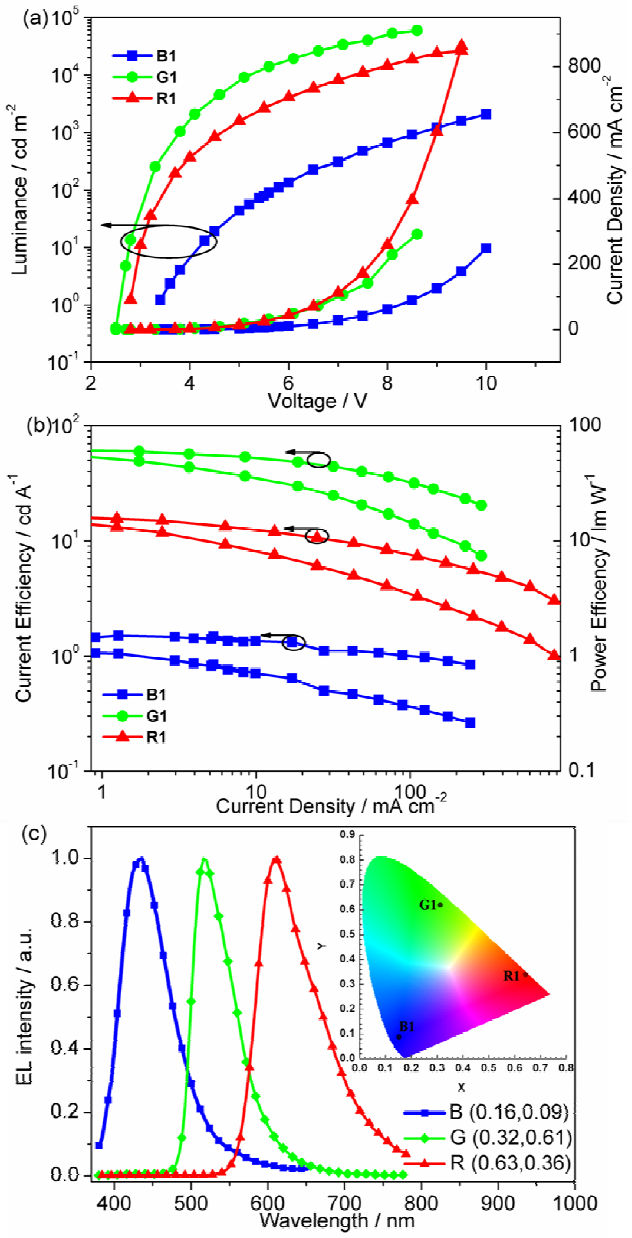

Fig. 8 (a) Current density–voltage–brightness (*J*–*V*–*L*) characteristics, (b) current efficiencies and power efficiencies versus current density curves and (c) electroluminescence (EL) spectra and CIE1931 coordinates for devices **B1**, **G1** and **R1** based on DPO-PPI.

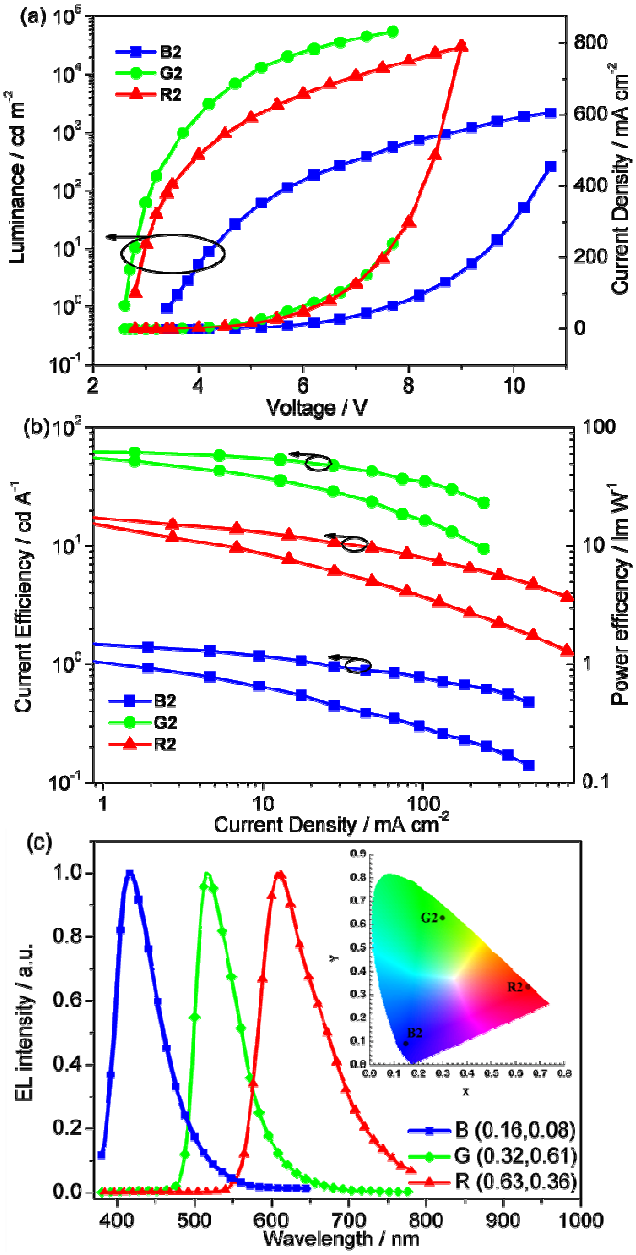

Fig. 9 (a) Current density–voltage–brightness (*J*–*V*–*L*) characteristics, (b) current efficiencies and power efficiencies versus current density curves and (c) electroluminescence (EL) spectra and CIE1931 coordinates for devices **B2**, **G2** and **R2** based on DPO-2PPI.

Cite this: DOI: 10.1039/c0xx00000x

www.rsc.org/xxxxxx

ARTICLE TYPE

Table 2 Electroluminescent properties of the devices.[a]

	Dopant	V_{on}/V	L_{max}/cd m^{-2}	η_c[b]/cd A^{-1}	η_p[b]/lm W^{-1}	η_{ext}[b]/%	CIE (x,y)[c]
B1	-	3.4	2077	1.51, 1.36, 1.01	1.29, 0.76, 0.38	1.88, 1.32, 0.79	0.16,0.09
B2	-	3.4	2178	1.75, 1.21, 0.71	1.53, 0.67, 0.26	2.24, 1.92, 1.42	0.16,0.08
G1	Ir(ppy)$_3$	2.6	55499	62.6, 61.6, 59.3	70.2, 61.4, 49.6	17.2, 17.1, 16.4	0.32,0.61
G2	Ir(ppy)$_3$	2.6	59310	65.4, 63.9, 61.8	73.3, 64.7, 52.2	18.0, 17.5, 16.9	0.30,0.63
R1	(bt)$_2$Ir(dipda)	2.6	26239	17.9, 16.2, 12.9	19.9, 14.6, 8.64	12.7, 11.5, 9.18	0.63,0.36
R2	(bt)$_2$Ir(dipda)	2.6	29245	19.0, 17.3, 13.8	21.3, 15.8, 9.57	13.5, 12.0, 9.65	0.63,0.36

[a]Abbreviation: V_{on}: Turn-on voltage. L_{max}: Maximum luminance. η_c: The maximum current efficiency. η_p: The maximum power efficiency. η_{ext}: The maximum external quantum efficiency. [b]in the order of maximum, then values at 100 and 1000 cd m^{-2}. [c]Measure at 100 cd m^{-2}

($\eta_{p.max}$) efficiencies of this device are 2.24%, 1.75 cd A^{-1} and 1.53 lm W^{-1}, respectively. Device **B1** using DPO-PPI as emitter showed slightly lower performance compared with device **B2** (Table 2).

Phosphorescent OLEDs

To evaluate the practical utility of DPO-PPI and DPO-2PPI as host materials, we fabricated devices with the following configurations: [ITO/MoO_3 (10 nm)/NPB (30 nm)/TCTA (5 nm)/DPO-PPI or DPO-2PPI:Ir(ppy)$_3$ (25 nm)/Bepp$_2$ (60 nm)/LiF (1 nm)/Al (100 nm)] (devices **G1** and **G2**) and [ITO/MoO_3 (10 nm)/NPB (30 nm)/TCTA (5 nm)/DPO-PPI or DPO-2PPI: (bt)$_2$Ir(dipba) (25 nm)/Bepp$_2$ (60 nm)/LiF (1 nm)/Al (100 nm)] (devices **R1** and **R2**). In these devices, green emissive Ir(ppy)$_3$ and red emissive (bt)$_2$Ir(dipba)[20] were doped in DPO-PPI and DPO-2PPI to form the emitting layer with optimized doping concentration of 8 wt% for Ir(ppy)$_3$ and (bt)$_2$Ir(dipba), respectively. Figure 7 presents energy level diagram of the used materials and molecular structures of the phosphorescent dyes Ir(ppy)$_3$ and (bt)$_2$Ir(dipba). The current density–voltage–brightness (*J*–*V*–*L*) characteristics, current efficiencies and power efficiencies versus current density curves of devices, and EL spectra of the devices are shown in Figure 8 and 9. All the devices performances are summarized in Table 2.

Both devices **G1** and **G2** show a turn-on voltage of 2.6 V. Device **G1** using DPO-PPI as host achieves a maximum current efficiency ($\eta_{c,max}$) of 62.6 cd A^{-1}, a maximum power efficiency ($\eta_{p,max}$) of 70.2 lm W^{-1}, and a maximum external quantum efficiency ($\eta_{ext,max}$) of 17.2%. In comparison, device **G2** hosted by DPO-2PPI exhibits slightly higher performance with $\eta_{c,max}$ of 65.4 cd A^{-1}, $\eta_{p,max}$ of 73.3 lm W^{-1}, and $\eta_{ext,max}$ of 18.0% (Figure 9 and Table 2). At practical brightness of 100 cd m^{-2}, the efficiencies are 61.6 cd A^{-1}, 61.4 lm W^{-1} and 17.1% for device **G1** and 63.9 cd A^{-1}, 64.7 lm W^{-1} and 17.5% for device **G2**. It is worth noting that device **G1** and **G2** show a low efficiencies roll-off. For example, when the brightness reaches 1000 cd m^{-2}, the device **G2** exhibits η_c of 61.8 cd A^{-1}, η_p of 52.2 lm W^{-1}, and η_{ext} of 16.9% without significant decay. Even when the brightness reaches as high as 10000 cd m^{-2}, η_c was still maintained as high as 50.3 cd A^{-1} (η_{ext} = 13.9%), which can be explained by the balance of charge carriers, as depicted in single-carrier devices, leading to a broad distribution of recombination within the emitting layer.[21] Although the EML of **G1** exhibits more balanced carrier-transporting ability than that of **G2**, device **G2** exhibits slightly better performance. A possible explanation is that as we know, the hole carriers are excessive than electron carriers in most devices. Therefore, the ability of electron-transporting of the EML may have a greater impact on device performance. The EML of **G2** shows slightly higher electron-transport ability than that of **G1**, which may lead to more balanced hole/electron current of the whole device, and thus benefits the device performance. These device performance, are comparable and attractive for the green phosphorescent OLEDs based on Ir(ppy)$_3$ reported to date.[4]

Next, the red-emitting OLEDs were fabricated using (bt)$_2$Ir(dipba) as dopant. Excellent performance and low efficiencies roll-off of red electrophosphorescense were obtained for devices **R1** and **R2** (Table 2). Device **R2** exhibited a higher maximum brightness of 29245 cd m^{-2}, at 9 V and maximum EL efficiencies (19.0 cd A^{-1}, 21.3 lm W^{-1}, 13.5%) with CIE coordinates of (0.63, 0.36). Device **R1** achieved a maximum brightness of 26239 cd m^{-2}, at 9.5 V and maximum EL efficiencies (17.9 cd A^{-1}, 19.9 lm W^{-1}, 12.7%) with CIE (0.63, 0.36). These devices displayed relatively pure red emission and there is no residual emission from the host and/or adjacent layers, indicating that the electroluminescence is solely from the phosphorescent dopants with completed energy transfer from host to dopant. Similar to the green-emitting devices **G1** and **G2**,

Given the similar frontier energy levels, the main efficiency difference should be ascribed to the different carrier injecting/transporting ability in EMLs. The non-doped and phosphorescent dyes-doped films based on DPO-2PPI show slightly higher electron injection/transport ability than those of DPO-PPI, thereby meaning more opportunity for carrier recombination in the EML. Besides, the triplet energy of DPO-2PPI (2.55 eV) is slightly lower than that of DPO-PPI (2.57 eV), which can reduce the loss of the energy transfer between the host and phosphorescent dopant and thus benefit the device performance. All these factors lead to the slightly higher device performance of DPO-2PPI than that of DPO-PPI. The remarkable performances for different emission color (R, G, B) were achieved from the essentially identical device architecture and incorporation of different phosphors, which make them very attractive for commercial applications in full color displays.

Conclusions

In summary, two DPO *meta*-substituted phenanthroimidazole derivatives, DPO-PPI and DPO-2PPI, were designed and synthesized to investigate the influence of the DPO moiety substitution on chemical, physical and electronic properties. With the saturation point of P=O group, the triplet energy of the chromophore PPI is almost preserved. Meanwhile, the emission of the films red shift to deep blue region due to the strong intermolecular interactions. The thermal stability and carrier injection/transport ability have been greatly improved after appending the DPO moiety. Moreover, they exhibited balanced carrier injection/transport ability in non-doped films and phosphorescent emitters-doped films. The two compounds were not only used as deep-blue emitters to fabricate non-doped deep-blue OLEDs, but also as phosphorescent host materials to construct highly efficient green and red PhOLEDs, accompanied with low efficiency roll-off characteristic. Therefore, high-performance three primary color (R, G and B) OLEDs have been achieved through a simple material system and identical device architecture, which is very meaningful and attractive for commercial application of full-color display and white lighting. Further application of the new compound in WOLEDs is ongoing in our lab.

Experimental

General Information

^{1}H NMR spectra were measured on Varian Mercury 300 MHz spectrometer with tetramethylsilane as the internal standard. Mass spectra were recorded on a Shimadzu AXIMA-CFR MALDITOF mass spectrometer. Elemental analyses were performed on a flash EA 1112 spectrometer. UV-vis absorption spectra were recorded spectra were recorded by a Shimadzu RF-5301 PC spectrometer. The absolute fluorescence quantum yields of solutions, films and solids were measured on Edinburgh FLS920 steady state fluorimeter (excited at 365nm). Differential scanning calorimetric (DSC) measurements were performed on a NETZSCH DSC204 instrument at a heating rate of 10 °C min^{-1} from 20 to 420 °C under a nitrogen atmosphere. Thermogravimetric analyses (TGA) were performed on a TA Q500 thermogravimeter by measuring their weight loss while heating at a rate of 10 °C min^{-1} from 25 to 800 °C under nitrogen. Electrochemical measurements were performed with a BAS 100W Bioanalytical electrochemical work station, using Pt as working electrode, platinum wire as auxiliary electrode, and a porous glass wick Ag/Ag$^+$ as pseudo-reference electrode with standardized against ferrocene/ferrocenium. The oxidation and reduction potentials were measured in CH_2Cl_2 and DMF solution containing 0.1 M of *n*-Bu_4NPF_6 as a supporting electrolyte at a scan rate of 200 mV s^{-1}.

Single Crystal Structure: The single crystal suitable for X-ray structural analysis was obtained by slow solution evaporation. Diffraction data were collected on a Rigaku RAXIS-PRID diffractometer using the ω-scan mode with graphite-monochromator Mo•Kα radiation. The structure was solved with direct methods using the SHELXTL programs and refined with full-matrix least-squares on F^2.[22] Non-hydrogen atoms were refined anisotropically. The positions of hydrogen atoms were calculated and refined isotropically. The corresponding CCDC reference number (CCDC**: 970126**) and the data can be obtained free of charge from The Cambridge Crystallographic Data Centre via www.ccdc.cam.ac.uk/data_request/cif.

Preparation of Materials: Tetrabutylammonium hexafluorophosphate (Bu_4NPF_6) was purchased from Aldrich. bis(2-(2-hydroxyphenyl)-pyridine)beryllium ($Bepp_2$), 1,4-bis[(1-naphthylphenyl)amino]-biphenyl (NPB) and 4,4′,4″-tri(*N*-carbazolyl)triphenylamine (TCTA) were prepared and purified by sublimation prior to use. All commercially available reagents were used as received unless otherwise stated. All reactions were carried out using Schlenk techniques under a nitrogen atmosphere. Compound PPI and 2-(3-bromophenyl)-1-phenyl-1*H*-phenanthro[9,10-*d*]imidazole was prepared according to previously reported procedures.[23]

*1-phenyl-2-(3-(diphenylphosphineoxide)phenyl)-1H-phenanthro[9,10-d]imidazole (*DPO-PPI*)*

To a solution of 2-(3-bromophenyl)-1-phenyl-1*H*-phenanthro[9,10-*d*]imidazole (0.90 g, 2 mmol) in THF (30 mL) was added n-BuLi (2.5 M in hexane, 0.88 mL) dropwise slowly at -78 °C. The solution was stirred at this temperature for 3 h, followed by addition of a solution of chlorodiphenylphosphine (0.56 g, 2.19 mmol) under nitrogen atmosphere. The resulting mixture was gradually warmed to ambient temperature and quenched by methanol (15 mL). The mixture was extracted with dichloromethane. The combined organic layers were dried magnesium sulfate, filtered, and evaporated under reduced pressure. The crude phoshphine was purified by column chromatography (silica, CH_2Cl_2) as white powder (776 mg, yield: 70%). Then the crude intermediate (550 mg, 1 mmol), dichloromethane (10 mL), and hydrogen peroxide (1.2 mL, 10 mmol, 30 %) were stirred overnight at room temperature. The organic layer was separated and washed with dichloromethane and water. The extract was evaporated to dryness affording a white solid and the crude product was purified by the train sublimation method (514 mg, yield: 90%). ^{1}H NMR (300 MHz, DMSO-d_6, δ): 8.92 (d, J = 8.1 Hz, 1H, Ar H), 8.87 (d, J = 8.4 Hz, 1H, Ar H), 8.66 (d, J = 7.8 Hz, 1H, Ar H), 7.95 (d, J = 7.8 Hz, 1H, Ar H), 7.77 (t, J = 7.5 Hz, 1H, Ar H), 7.72 – 7.53 (m, 16H, Ar H), 7.49 – 7.42 (m, 4H, Ar H), 7.32 (t, J = 7.5 Hz, 1H, Ar H), 7.02 (d, J = 8.4 Hz, 1H, Ar H). ^{13}C NMR (125 MHz, $CDCl_3$): δ 149.82, 138.27, 133.40, 133.17, 132.50, 132.18, 132.10, 132.01, 131.76, 130.21, 129.86, 129.42, 129.08, 128.98, 128.90, 128.59, 128.49, 128.38, 128.35, 127.40, 127.10, 126.35, 125.81, 125.14, 124.15, 123.16, 122.88, 122.71, 120.82. MALDI-TOF-MS(M): m/z: 570.9 [M]$^+$ (calcd: 570.2). Anal. Calcd (100%) for $C_{39}H_{27}N_2OP$: C 82.09, H 4.77, N 4.91; found: C 82.47, H 4.62, N 4.89.

*1-phenyl-2-(3-(phenyl(3-(1-phenyl-1H-phenanthro[9,10-d]imidazol-2-yl)phenyl)phosphineoxide)phenyl)-1H-phenanthro[9,10-d]imidazole (*DPO-2PPI*)*

To a solution of 2-(3-bromophenyl)-1-phenyl-1*H*-phenanthro[9,10-*d*]imidazole (2.04 g, 4.5 mmol) in THF (30 mL) was added n-BuLi (2.5 M in hexane, 2 mL) dropwise slowly at -78 °C. The solution was stirred at this temperature for 3 h, followed by addition of a solution of dichloro(phenyl)phosphine (0.27 g, 1.5 mmol) under nitrogen atmosphere. The resulting yellow solution was gradually warmed to ambient temperature and quenched by methanol (30 mL). The mixture was extracted

with dichloromethane. The combined organic layers were dried magnesium sulfate, filtered, and evaporated under reduced pressure. The crude phoshphine was purified by column chromatography (silica, CH_2Cl_2/ethyl acetate = 20 : 1) as deep blue powder (2.06 g, yield: 54%). Then the crude intermediate (430 mg, 0.5 mmol), dichloromethane (10 mL), and hydrogen peroxide (0.4 mL, 3 mmol, 30%) were stirred overnight at room temperature. The organic layer was separated and washed with dichloromethane and water. The extract was evaporated to dryness affording a yellowish solid and the crude product was purified by the train sublimation method (353 mg, yield: 82%). ^{1}H NMR (300 MHz, DMSO-d_6, δ): 8.93 (d, J = 8.4 Hz, 2H, Ar H), 8.87 (d, J = 8.4 Hz, 2H, Ar H), 8.68 – 8.65 (m, 2H, Ar H), 7.97 (d, J = 7.8 Hz, 2H, Ar H), 7.74 – 7.26 (m, 29H, Ar H), 7.02 (d, J = 7.5 Hz, 2H, Ar H). ^{13}C NMR (125 MHz, $CDCl_3$): δ 149.75, 138.18, 137.43, 133.34, 132.76, 132.47, 132.20, 132.12, 130.25, 129.96, 129.42, 128.97, 128.84, 128.58, 128.37, 127.41, 127.11, 126.38, 125.80, 125.16, 124.13, 123.17, 122.87, 122.72, 120.84. MALDI-TOF-MS(M): m/z: 862.2 $[M]^+$ (calcd: 862.9). Anal. Calcd (100%) for $C_{60}H_{39}N_4OP$: C 83.51, H 4.56, N 6.49; found: C 83.29, H 4.50, N 6.42.

Theoretical Calculations: The ground state geometries were fully optimized by the density functional theory (DFT)[24] method with the Becke three-parameter hybrid exchange and the Lee-Yang-Parr correlation functional[25] (B3LYP) and 6-31G* basis set using the Gaussian 03 software package.[26]

Device Fabrication and Measurement: Before device fabrication, the ITO glass substrates were pre-cleaned carefully and treated by UV/O_3 for 2 min. Then the sample was transferred to the deposition system. The devices were prepared in vacuum at a pressure of 5 × 10^{-6} Torr. The hole-injection material MoO_3, hole-transporting material NPB (1,4-bis(1-naphthylphenylamino)-biphenyl), exciton blocking material TCTA (4,4′,4″-tri(*N*-carbazolyl)triphenylamine), hole-blocking and electron-transporting material $Bepp_2$ (bis(hydroxyphenyl-pyridine) beryllium) were commercially available and thermally evaporated at a rate of 1.0 Å s^{-1}. After the organic film deposition, 1 nm of LiF and 100 nm of aluminum were thermally evaporated onto the organic surface. The thicknesses of the organic materials and the cathode layers were controlled using a quartz crystal thickness monitor. All of used organic materials have been purified by vacuum sublimation approach. The electrical characteristics of the devices were measured with a Keithley 2400 source meter. The EL spectra and luminance of the devices were obtained on a PR650 spectrometer. All the devices fabrication and device characterization steps were carried out at room temperature under ambient laboratory conditions. Current-Voltage characteristics of single-carrier devices were measured using the same semiconductor parameter analyzer as for PhOLED devices. The single-carrier devices measurements were performed under dark and ambient conditions.

Acknowledgements

This work was supported by National Basic Research Program of China (2013CB834805), National Natural Science Foundation of China (51173064, 91333201 and 51373062) and Program for Chang Jiang Scholars and Innovative Research Team in University (No.IRT13018).

Notes and references

*State Key Laboratory of Supramolecular Structure and Materials College of Chemistry, Jilin University, Changchun 130012, P. R. China E-mail:*yuliu@jlu.edu.cn (Y. Liu); yuewang@jlu.edu.cn (Y. Wang)

† Electronic Supplementary Information (ESI) available: [photophysical property of compound PPI under same condition]. See DOI: 10.1039/b000000x/

1 C. W. Tang and S. A. VanSlyke, *Appl. Phys. Lett.*, 1987, **51**, 913.

2 (a) K. T. Kamtekar, A. P. Monkman and M. R. Bryce, *Adv. Mater.*, 2010, **22**, 572; (b) G. M. Farinola and R. Ragni, *Chem. Soc. Rev.*, 2011, **40**, 3467; (c) S. Reineke, F. Lindner, G. Schwartz, N. Seidler, K. Walzer, B. Lüssem, K. Leo, *Nature* 2009, **459**, 234; (d) A. C. Grimsdale, K. L. Chan, R. E. Martin, P. G. Jokisz, A. B. Holmes, *Chem, Rev.,* 2009, **109**, 897.

3 (a) Y. Tao, Q. Wang, C. Yang, Q. Wang, Z. Zhang, T. Zou, J. Qin and D. Ma, *Angew. Chem., Int. Ed.,* 2008, **120**, 8224; (b) Y. Y. Lyu, J. Kwak, W. S. Jeon, Y. Byun, H. S. Lee, D. Kim, C. Lee and K. Char, *Adv. Funct. Mater.,* 2009, **19**, 420; (c) J. Kwak, Y. Lyu, H. Lee, B. Choi, K. Char and C. Lee, *J. Mater. Chem.,* 2012, **22**, 6351; (d) C. H. Fan, P. P. Sun, T. H. Su, C. H. Cheng, *Adv. Mater.,* 2011, **23**, 2981; (e) D. H. Kim, N. S. Cho, H. Y. Oh, J. H. Yang, W. S. Jeon, J. S. Park, M. C. Suh, J. H. Kwon, *Adv. Mater.,* 2011, **23**, 2721; (f) H. H. Chou, C. H. Cheng, *Adv. Mater.,* 2010, **22**, 2468; (g) H. Fukagawa, T. Shimizu, H. Hanashima, Y. Osada, M. Suzuki, H. Fujikake, *Adv. Mater.,* 2012, **24**, 5099; (h) Y. Cho, J. Lee, *Adv. Mater.,* 2011, **23**, 4568.

4 (a) H. Huang, Y. Wang, B. Wang, S. Zhuang, B. Pan, X. Yang, L. Wang, C. Yang, *J. Mater. Chem. C*, 2013, **1**, 5899; (b) H-F. Chen, S-J. Yang, Z-H. Tsai, W-Y. Hung, T-C. Wang, K-T. Wong, *J. Mater. Chem.,* 2012, **22**, 6351; (c) Y. Zhu, L. Zhou, H. Li, Q. Xu, M. Teng, Y. Zheng, J. Zuo, H. Zhang, X. You, *Adv. Mater.,* 2011, **23**, 4041; (d) C-H. Chang, M.-C. Kuo, W.-C. Lin, Y.-T Chen, K.-T. Wong, S.-H. Chou, E. Mondal, R. C. Kwong, S. Xia, T. Nakagawa, C. Adachi, *J. Mater. Chem.,* 2012, **22**, 3832; (e) M. Hashimoto, S. Igawa, M. Yashima, I. Kawata, M. Hoshino, M. Osawa, *J. Am. Chem. Soc.,* 2011, **133**, 10348; (f) S. Gong, Y. Zhao, C. Yang, C. Zhong, J. Qin, D. Ma, *J. Phys. Chem. C,* 2010, **114**, 5193; (g) Y. Tao, Q. Wang, C. Yang, C. Zhong, K. Zhang, J. Qin, D. Ma, *Adv. Funct. Mater.,* 2009, **19**, 1.

5 (a) Y. Wei and C. T. Chen, *J. Am. Chem. Soc.,* 2007, **129**, 7478; (b) Z. Jiang, Z. Liu, C. Yang, C. Zhong, J. Qin, G. Yu, Y. Liu. *Adv. Funct. Mater.,* 2010, **12**, 452; (c) C. Zheng, W. Zhao, Z. Wang, D. Huang, J. Ye, X. Qu, X. Zhang, C. Lee, S. Lee. *J. Mater. Chem.,* 2010, **20**, 1560; (d)Y. Zhang, S. L. Lai, Q. X. Tong, M. F. Lo, T. W. Ng, M. Y. Chan, Z. C. Wen, J. He, K. S. Jeff, X. L. Tang, W. M. Liu, C. C. Ko, P. F. Wang, C. S. Lee, *Chem. Mater.,* 2012, **24**, 61; (e) S. Gong, Y. Zhao, M. Wang, C. Yang, C. Zhong, J. Qin, D. Ma, *Chem. Asian J.* 2010, **5**, 2093; f) S. K. Kim, B. Yang, Y. Ma, J. H. Leec, J. Park, *J. Mater. Chem.*, 2008, **18**, 3376; (g) D. Thirion, M. Romain, J. Rault-Berthelot, C. Poriel, *J. Mater. Chem.,* 2012, **22**, 7149; (h) C. Poriel, N. Cocherel, J. Rault-Berthelot, L. Vignau, O. Jeannin, *Chem. Eur. J.,* 2011, **17**, 12631; (i) A. L. Fischer, K. E. Linton, K. T. Kamtekar, C. Pearson, M. R. Bryce, M. C. Petty, *Chem. Mater.,* 2011, **23**, 1640; (j) K. E. Linton, A. L. Fischer, C. Pearson, M. A. Fox, L.-O. Palsson, M. R. Bryce, M. C. Petty, *J. Mater. Chem.,* 2012, **22**, 11816; (k) X. Xing, L. Xiao, L. Zheng, S. Hu, Z. Chen, B. Qu, Q. Gong, *J. Mater. Chem.,* 2012, **22**, 15136; (l) M. Zhu, Q. Wang, Y. Gu, X. Cao, C. Zhong, D. Ma, J. Qin, C. Yang, *J. Mater. Chem.,* 2011, **21**, 6409; (m) Y. Yuan, J. Chen, F. Lu, Q. Tong, Q. Yang, H. Mo, T. Ng, F. Wong, Z. Guo, J. Ye, Z. Chen, X. Zhang, C. Lee, *Chem. Mater.,* 2013, **25**, 4957.

6 (a) J. Kwon, S. Park, S. Y. Park, *J. Am. Chem. Soc.*,2013, **135**, 11239; (b) S. Xue, L. Yao, C. Gu, H. Zhang, F. Shen, Z. Xie, H. Wu, Y. Ma, *J. Mater. Chem. C*, 2013, **1**, 7175; (c) W.-C. Lin, W.-C. Huang, M.-H. Huang, C.-C. Fan, H.-W. Lin, L.-Y. Chen, Y.-W. Liu, J.-S. Lin, T.-C. Chao, M.-R. Tseng, *J. Mater. Chem. C*, 2013, **1**, 6835; (d) S. Dong, Y. Liu, Q. Li, L. Cui, H. Chen, Z. Jiang, L. Liao, *J. Mater. Chem. C*, 2013, **1**, 6575; (e) S. Chen, G. Tan, W-Y. Wong, H-S. Kwok, *Adv. Funct. Mater.* 2011, **21**, 3785; (f) G. M. Farinola, R.

Ragni, *Chem. Soc. Rev.* 2011, **40**, 3467; (g) S. L. Gong, Y. H. Chen, J. J. Luo, C. L. Yang, C. Zhong, J. G. Qin, D. G. Ma, *Adv. Funct. Mater.,* 2011, **21**, 1168; (h) B. P. Yan, C. C. C. Cheung, S. C. F. Kui, H. F. Xiang, V. A. L. Roy, S. J. Xu, C. M. Che, *Adv. Mater.,* 2007, **19**, 3599; (i) H. Sasabe, J. I. Takamatsu, T. Motoyama, S. Watanabe, G. Wagenblast, N. Langer, O. Molt, E. Fuchs, C. Lennartz, J. Kido, *Adv. Mater.,* 2010, **22**, 5003; (j) R. J. Wang, D. Liu, H. C. Ren, T. Zhang, H. M. Yin, G. Y. Liu, J. Y. Li, *Adv. Mater.,* 2011, **23**, 2823; (k) K. T. Kamtekar, A. P. Monkman, M. R. Bryce, *Adv. Mater.,* 2010, **22**, 572; (l) M. C. Gather, A. Köhnen, K. Meerholz, *Adv. Mater.,* 2011, **23**, 233; (m) S. Dong, Y. Liu, Q. Li, L. Cui, H. Chen, Z. Jiang, L. Liao, *J. Mater. Chem. C*, 2013, **1**, 6575.

7 (a) X. Liu, C. Zheng, M. Lo, J. Xiao, C. Lee, M. Fung, X. Zhang, *Chem. Commun*., 2014, **50**, 2027; (b) H. Huang, Y. Wang, B. Pan, X. Yang, L. Wang, J. Chen, D. Ma, C. Yang, *Chem. Eur. J.* 2013, **19**, 1828; (c) W. Hung, L. Chi, W. Chen, Y. Chen, S. Chou, K. Wong, *J. Mater. Chem.*, 2010, **20**, 10113; (d) B. Pan, B. Wang, Y. Wang, P. Xu, L. Wang, J. Chen, D. Ma, *J. Mater. Chem. C*, 2014, **2**, 2466; (e) X. Liu, C. Zheng, M. Lo, J. Xiao, Z. Chen, C. Liu, C. Lee, M. Fung, X. Zhang, *Chem. Mater.*, 2013, **25**, 4454.

8 (a) L. Duan, J. Qiao, Y. Sun, Y. Qiu, *Adv. Funct. Mater.*, 2011, **23**, 1137; (b) Y. Tao, C. Yang, J. Qin, *Chem. Soc. Rev.*, 2011, **40**, 2943.

9 K. Wang, F. Zhao, C. Wang, S. Chen, D. Chen H. Zhang, Y. Liu, D. Ma, Y. Wang, *Adv. Funct. Mater.*, 2013, **23**, 2672.

10 (a) A. B. Padmaperuma, L. S. Sapochak, P. E. Burrows, *Chem. Mater.* 2006, **18**, 2389; (b) D. Yu, F. Zhao, Z. Zhang, C. Han, H. Xu, J. Li, D. Ma, P. Yan, *Chem. Commun.*, 2012, **48**, 6157.

11 P. Calcagno, B. M. Kariuki, S. J. Kitchin, J. Robinson, D. Philp, K. D. M. Harris, *Chem. Eur. J.* 2000, **6**, 2338.

12 (a) S. O. Jeon, K. S. Yook, C. W. Joo, J. Y. Lee, *Adv. Funct. Mater.* 2009, **19**, 3644; (c) P. A. Vecchi, A. B. Padmaperuma, H. Qiao, L. S. Sapochak, P. E. Burrows, *Org. Lett.* 2006, **8**, 4211; (d) F.-M. Hsu, C.-H. Chien, P. I. Shih, C. F. Shu, *Chem. Mater.* 2009, **21**, 1017; (e) E. Polikarpov, J. S. Swensen, N. Chopra, F. So, A. B. Padmaperuma, *Appl. Phys. Lett.* 2009, **94**, 223304; (f) S. E. Jang, C. W. Joo, S. O. Jeon, K. S. Yook, J. Y. Lee, *Org. Electron.* 2010, **11**, 1059; (g) J. Lee, J.-I. Lee, J. Y. Lee, H. Y. Chu, *Appl. Phys. Lett.* 2009, **95**, 253304; (h) J. Lee, J. I. Lee, J. Y. Lee, H. Y. Chu, *Org. Electron.* 2009, **10**, 1529; (i) H.- H. Chou, C.-H. Cheng, *Adv. Mater.* 2010, **22**, 2468. (j) C. Han, Z. Zhang, H. Xu, S. Yue, J. Li, P. Yan, Z. Deng, Y. Zhao, P. Yan, S. Liu, *J. Am. Chem. Soc.*,2012, **134**, 19179.

13 (a) C. Han, G. Xie, H. Xu, Z. Zhang, D. Yu, Y. Zhao, P. Yan, Z. Deng, Q. Li, S. Liu, *Chem. Eur. J.,* 2011, **17**, 445; (b) A. Wada, T. Yasuda, Q. Zhang, Y. S. Yang, I. Takasu, S. Enomoto, C. Adachi, *J. Mater. Chem. C*, 2013, **1**, 2404; (c) D. Yu, Y. Zhao, H. Xu, C. Han, D. Ma, Z. Deng, S. Gao, P. Yan, *Chem. Eur. J.,* 2011, **17**, 2592; (d) C. Fan, F. Zhao, P. Gan, S. Yang, T. Liu, C. Zhong, D. Ma, J. Qin, C. Yang, *Chem. Eur. J.,* 2012, **18**, 5510; (e) J. Zhao, G. Xie, C. Yin, L. Xie, C. Han, R. Chen, H. Xu, M. Yi, Z. Deng, S. Chen, Y. Zhao, S. Liu, W. Huang, *Chem. Mater.,* 2011, **23**, 5331; (f) W. Jiang, L. Duan, J. Qiao, G. Dong, L. Wang, Y. Qiu, *Org. Lett.,* 2011, **13**, 3146; (g) D. Yu, F. Zhao, C. Han, H. Xu, J. Li, Z. Zhang, Z. Deng, D. Ma, P. Yan, *Adv. Mater.,* 2012, **24**, 509; (h) C. Han, Z. Zhang, H. Xu, J. Li, G. Xie, R. Chen, Y. Zhao, W. Huang, *Angew. Chem. Int. Ed.,* 2012, **51**, 10104; (i) S. O. Jeon, K. S. Yook, C. W. Joo, J. Y. Lee, *Adv. Mater.*, 2010, **22**, 1872.

14 (a) Y. Shirota, *J. Mater. Chem.,* 2000, **10**, 1; (b) C. Adachi, K. Nagai, N. Tamoto, *Appl. Phys. Lett.* 1995, **66**, 2679.

15 C. M. Cardona, W. Li, A. E. Kaifer, D. Stockdale, M. and G. C. Bazan, *Adv. Mater.,* 2011, **23**, 2367.

16 (a) C. J. Zheng, J. Ye, M. F. Lo, M. K. Fung, X. M. Ou, X. H. Zhang and C. S. Lee, *Chem. Mater.,* 2012, **24**, 643; (b) F. M. Hsu, C. H. Chien, Y. J. Hsieh, C. H. Wu, C. F. Shu, S. W. Liu and C. T. Chen, *J. Mater. Chem.,* 2009, **19**, 8002; (c) S. J. Su, E. Gonmori, H. Sasabe and J. Kido, *Adv. Mater.*, 2008, **20**, 4189.

17 (a) Z. Ge, T. Hayakawa, S. Ando, M. Ueda, T. Akiike, H. Miyamoto, T. Kajita, M. Kakimoto, *Adv. Funct. Mater*., 2008, **18**, 584; (b) Z. Ge, T. Hayakawa, S. Ando, M. Ueda, T. Akiike, H. Miyamoto, T. Kajita, M. Kakimoto, *Chem. Mater*., 2008, **20**, 2532; (c) C. Fan, Y. Chen, Z. Jiang, C. Yang, C. Zhong, J. Qin, D. Ma, *J. Mater. Chem.,* 2010, **20**, 3232.

18 (a) Y. Shirota, H. Kageyama, *Chem. Rev.*, 2007, **107**, 953; (b) V. Coropceanu, J. Cornil, D. Filho, Y. Olivier, R. Silbey, J. Brédas, *Chem. Rev.*, 2007, **107**, 926.

19 (a) X. Qiao, Y. Tao, Q. Wang, D. Ma, C. Yang, L. Xiang, J. Qin, F. Wang, *J. Appl. Phys.* 2010, **108**, 034508; (b) F. Nuesch, D. Berner, E. Tutis, M. Schaer, C. Ma, X. Wang, B. Zhang, L. Zuppiroli, *Adv. Funct. Mater*., 2005, **15**, 323; (c) S. Zhang, S. Yue, Q. Wu, Z. Zhang, Y. Chen, X. Wang, Z. Liu, G. Xie, Q. Xue, D. Qu, Y. Zhao, S. Liu, *Org. Electron*., 2013, **14**, 2014.

20 T. Peng, H. Bi, Y. Liu, Y. Fan, H. Gao, Y. Wang and Z. Hou, *J. Mater. Chem.*, 2009, **19**, 8072.

21 (a) T. Komino, H. Nomura, T. Koyanagi, C. Adachi, *Chem. Mater.* 2013, **25**, 3038; (b) D. Wagner, S. T. Hoffmann, U. Heinemeyer, I. Münster, A. Köhler, P. Strohriegl, *Chem. Mater.* 2013, **25**, 3758.

22 SHELXTL, Version 5.1; Siemens Industrial Automation, Inc. **1997**; G. M. Sheldrick, SHELXS-97, Program for Crystal Structure Solution; University of Göttingen: Göttingen, **1997**.

23 (a) Y. Yuan, D. Li, X. Zhang, X. Zhao, Y. Liu, J. Zhang, Y. Wang, *New. J. Chem.,* 2011, **35**, 1534; (b) H. Huang, Y. Wang, S. Zhuang, X. Yang, L. Wang and C. Yang, *J. Phys. Chem. C,* 2012, **116**, 19458.

24 E. Runge, E. K. U. Gross, *Phys. Rev. Lett.,* 1984, **52**, 997.

25 A. D. J. Becke, *Chem. Phys.* 1993, **98**, 5648.

26 M. J. Frisch et al., *Gaussian 03*, *Revision C.02*, Gaussian, Inc.: *Pittsburgh, PA* **2003**.

Graphical Abatract:

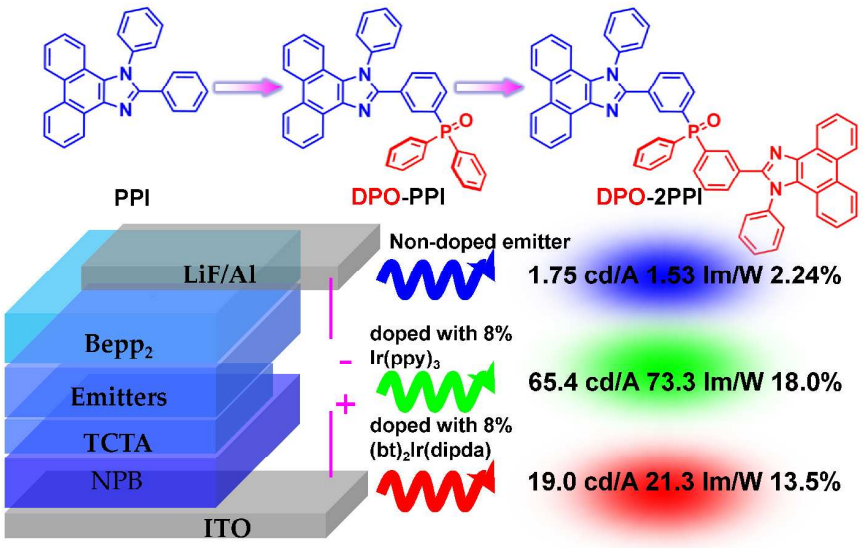

We here exhibited two novel phosphine oxide moiety attaching phenanthroimidazole hybrids. The appendent P=O moiety preserves the high triplet energy and endows the films with high quantum yields in deep-blue region n. It improves the carrier injection/transport ability greatly. The two complexes are used not only as emitters to fabricate high-performance deep-blue OLEDs (1.75 cd A^{-1}, 1.53 lm W^{-1}, 2.24%), but also as hosts to fabricate high-performance green PhOLEDs (65.4 cd A^{-1}, 73.3 lm W^{-1}, 18.0%) and red PhOLEDs (19.0 cd A^{-1}, 21.3 lm W^{-1}, 13.5%).